SCIENTIFIC REPORTS

OPEN

SUBJECT AREAS:
NANOPHOTONICS AND PLASMONICS
SUB-WAVELENGTH OPTICS
PHOTONIC DEVICES
NONLINEAR OPTICS

Received
28 October 2013

Accepted
24 December 2013

Published
17 January 2014

Correspondence and requests for materials should be addressed to X.Y.H. (xiaoyonghu@pku.edu.cn) or Q.H.G. (qhgong@pku.edu.cn)

On-chip plasmon-induced transparency based on plasmonic coupled nanocavities

Yu Zhu[1], Xiaoyong Hu[1,2], Hong Yang[1] & Qihuang Gong[1,2]

[1]State Key Laboratory for Mesoscopic Physics & Department of Physics, Peking University, Beijing 100871, People's Republic of China, [2]Collaborative Innovation Center of Quantum Matter, Beijing 100871, People's Republic of China.

On-chip plasmon-induced transparency offers the possibility of realization of ultrahigh-speed information processing chips. Unfortunately, little experimental progress has been made to date because it is difficult to obtain on-chip plasmon-induced transparency using only a single meta-molecule in plasmonic circuits. Here, we report a simple and efficient strategy to realize on-chip plasmon-induced transparency in a nanoscale U-shaped plasmonic waveguide side-coupled nanocavity pair. High tunability in the transparency window is achieved by covering the pair with different organic polymer layers. It is possible to realize ultrafast all-optical tunability based on pump light-induced refractive index change of a graphene cover layer. Compared with previous reports, the overall feature size of the plasmonic nanostructure is reduced by more than three orders of magnitude, while ultrahigh tunability of the transparency window is maintained. This work also provides a superior platform for the study of the various physical effects and phenomena of nonlinear optics and quantum optics.

Plasmon-induced transparency, which is a plasmonic analogue of classical electromagnetically induced transparency, has attracted enormous attention because of its potentially important applications in the fields of integrated photonic devices and ultrahigh-speed information processing chips. Various configurations have been presented to date to demonstrate plasmon-induced transparency effects in plasmonic nanostructures, such as the use of metamaterials[1–5], metallic photonic crystals[6–9], plasmonic resonators[10], and metallic bar gratings[11]. However, plasmon-induced transparency is generated only when these configurations are excited by a signal light that is incident in a direction that is nonparallel to the chip surface, i.e., off-chip plasmon-induced transparency[12]. Also, these structures contain large numbers of repeating meta-molecule units arranged in periodic arrays. However, the practical nanoscale devices that are to be used in photonic central processing unit (CPU) chips and quantum solid chips require on-chip plasmon-induced transparency, i.e., where the plasmon-induced transparency is excited by signal light that is incident in the direction parallel to the chip surface. While two methods, the phase-coupling mechanism[13,14] and the waveguide-microcavity coupling mechanism[15–18], have been proposed to demonstrate on-chip plasmon-induced transparency, very few experimental achievements have been reported to date. Part of the reason for this is that only a single planar meta-molecule can be used, so the significant phenomenon of on-chip plasmon-induced transparency is very difficult to obtain[19]. Also, the transmission contrast obtained between the transparency window center and the stop band was so low as to be less than 15%, and no tunable on-chip plasmon-induced transparency has been reported[19]. This has greatly restricted the practical applications of on-chip plasmon-induced transparency.

Here, we report a simple and effective strategy to realize high-contrast on-chip plasmon-induced transparency in a plasmonic waveguide side-coupled to a pair of closely arranged nanocavities. There is strong coupling between the two nanocavities when they are connected via the plasmonic waveguide. Therefore, we called this the 'plasmonic coupled nanocavities' configuration. A U-shaped plasmonic waveguide side-coupled nanocavity pair structure was adopted in our experiment. The remarkable features of the U-shaped plasmonic waveguide lie in its strong light-field localization, relatively low propagation losses, high transmission through sharp bends, and high tolerance for structural imperfections[20]. Verslegers *et al.* noted that the destructive interference between two excitation pathways that involve two nanocavities being side-coupled via a plasmonic waveguide can form a plasmon-induced transparency[21]. A powerful on-chip plasmon-induced transparency effect with high transmission contrast of over 60% was obtained. An ultrasmall feature size of the order of 100 nm was achieved for these plasmonic coupled nanocavities. The entire plasmonic nanostructure was reduced by more than three orders of

magnitude compared with previously reported off-chip plasmon-induced transparency structures, and was also reduced by more than one order of magnitude when compared with previously reported on-chip plasmon-induced transparency structures[1–12,19]. A high degree of tunability in the transparency window is achieved using different polymer cover layers. It is possible to realize ultrafast all-optical tunability based on pump light-induced refractive index change of a graphene cover layer. This work not only offers a way to realize integrated photonic devices and construct ultrahigh-speed information processing chips, but also provides an excellent platform for fundamental studies of nonlinear optics and quantum optics.

Results

Waveguiding properties of U-shaped plasmonic waveguides. The schematic structure of a U-shaped plasmonic waveguide is shown in Fig. 1(a). The U-shaped plasmonic waveguide consists of an infinitely-long air groove with a width of 150 nm and a depth of 150 nm etched in a 300-nm-thick gold film. The dispersion relations of the plasmonic waveguide were calculated using the finite element method (using the commercial software package COMSOL Multiphysics)[22], and the calculated results are shown in Fig. 1(b). The refractive index of air was set to be 1. The wavelength-dependent complex refractive index of gold was obtained from Ref. 23. The U-shaped plasmonic waveguide can offer wideband guided surface plasmon polariton (SPP) modes, which was confirmed by the calculations of Li *et al.*[24]. To further confirm these guided SPP modes, we calculated the power density profile of a guided mode excited by continuous wave (CW) incident light at a wavelength of 830 nm using the finite element method, and the calculated results are shown in Fig. 1(c). The guided mode is mainly confined within the groove region and extends slightly into the adjacent air regions. The maximum intensity is located at the gold-air interface around two vertexes in the upper side. This shows good agreement with the calculations of Li *et al.*[24]. To further confirm the SPP propagation properties, we also etched an 8-μm-long U-shaped plasmonic waveguide on a silicon dioxide substrate, as shown in Fig. 1(d). To efficiently excite and collect the required SPPs, we etched a nanoslit connected to a triangular air groove in the gold film in the input port of the U-shaped plasmonic waveguide. The

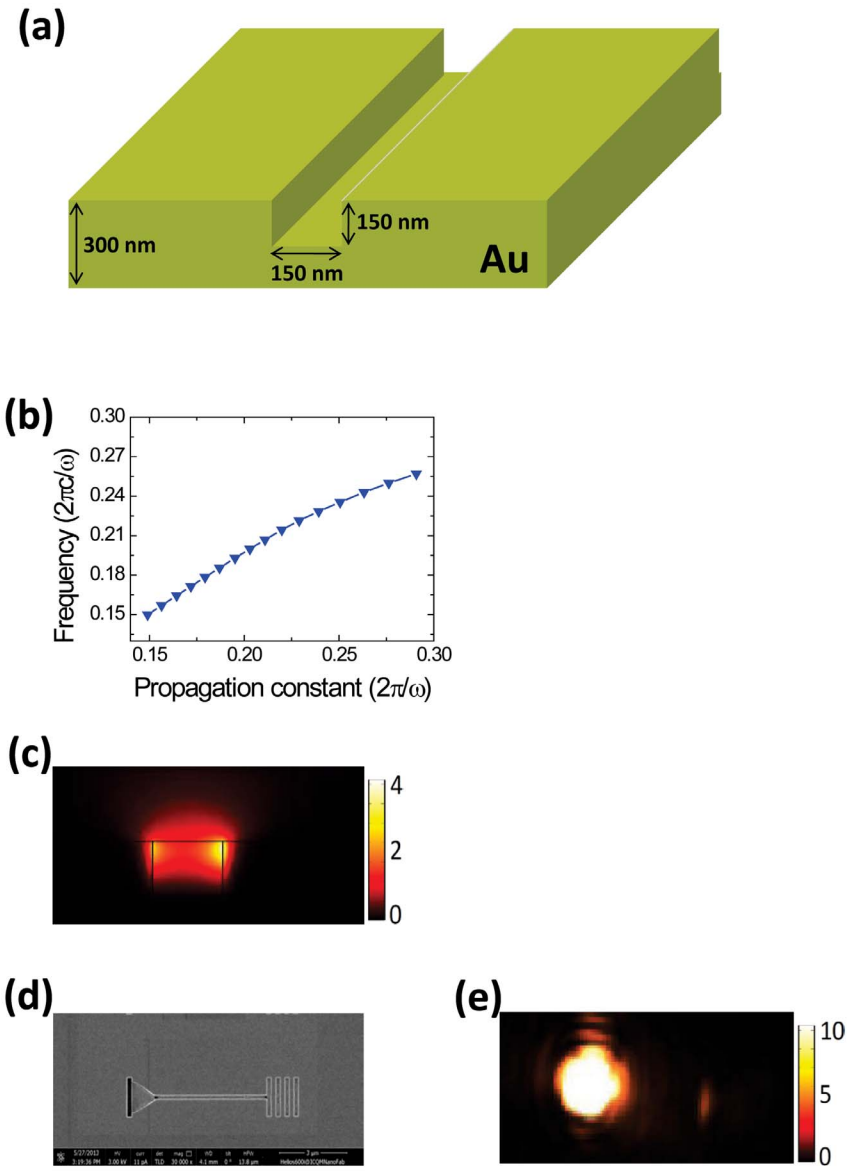

Figure 1 | Characterization of the U-shaped plasmonic waveguide. (a) Schematic structure. (b) Dispersion relations. (c) Power density profile of guided mode excited by incident CW light with a wavelength of 830 nm. (d) SEM image of an 8-μm-long U-shaped plasmonic waveguide. (e) Measured CCD image of an 8-μm-long U-shaped plasmonic waveguide under excitation by an 830-nm CW laser (e).

length, width, and depth of this nanoslit were 2 μm, 200 nm, and 300 nm, respectively. The depth of the triangular air groove was 150 nm. We also etched a grating in the output port to help to couple the guided SPP modes into free space for measurement purposes. Under excitation by a CW laser beam at a wavelength of 830 nm, remarkable scattered light was output from the decoupling grating, as shown in Fig. 1(e). This confirms the excellent propagation properties of the guided SPP modes.

On-chip plasmon-induced transparency performance. A schematic of the structure of the plasmonic coupled nanocavities is shown in Fig. 2(a), consisting of a long stub nanocavity and a short stub nanocavity that are side-coupled to a U-shaped plasmonic waveguide from the two lateral sides. The long stub nanocavity and the short stub nanocavity were closely arranged along the U-shaped plasmonic waveguide. The U-shaped plasmonic waveguide was composed of an air groove with a width of 150 nm and a depth of 150 nm that was etched into a 300-nm-thick gold film. The length, width, and depth of the long stub nanocavity were 150 nm, 150 nm, and 150 nm, respectively. The length, width, and depth of the short stub nanocavity were 110 nm, 150 nm, and 150 nm, respectively. The distance between the centers of the long nanocavity and the short nanocavity was 50 nm along the direction of the plasmonic waveguide. A top-view scanning electron microscopy (SEM) image of the plasmonic coupled nanocavities is shown in Fig. 2(b). Although

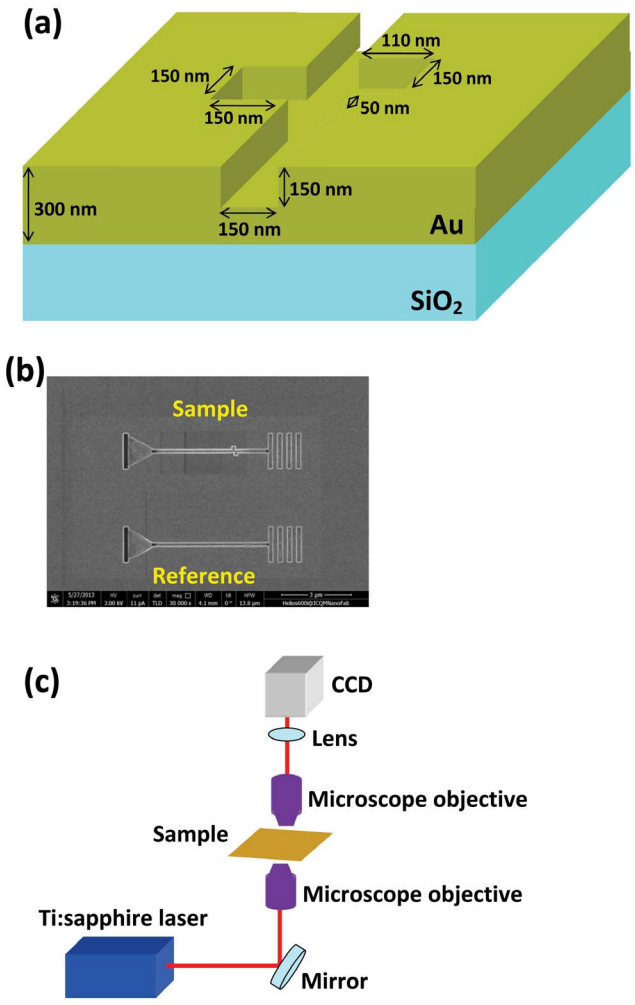

Figure 2 | Characterization of coupled nanocavities sample. (a) Schematic structure. (b) SEM image. (c) Schematic of the experimental set-up of the nano-spectroscopy measurement system.

the effective feature size was of the order of 100 nm, a long plasmonic waveguide with a length of 8 μm was used in our experiment for easy of measurement and characterization. A nanoslit connected via a triangular air groove was etched in the input port of the plasmonic waveguide to effectively excite and collect the required SPPs. A decoupling grating was also etched in the output port to scatter the SPPs into free space for measurement purposes. In our experiments, a nano-spectroscopy measurement system was used to study the transmission properties of the plasmonic coupled nanocavities. The measured linear transmission spectrum of the plasmonic coupled nanocavities is shown in Fig. 3(a). The linear transmission was normalized with respect to a reference waveguide, which was composed of an 8-μm-long U-shaped plasmonic waveguide with the same structural parameters as that of the sample, but without the two plasmonic nanocavities, which is a standard method that is widely used to study the on-chip transmission properties of plasmonic nanostructures[19]. Subject to the limits of the tunable wavelength range of the Ti:sapphire laser system, the linear transmission spectrum was measured from 780 to 980 nm. A sharp and high transmission peak appeared in the transmission forbidden band, implying the formation of plasmon-induced transparency. The destructive interference between two resonant excitation pathways related to the long and short nanocavities generates the plasmon-induced transparency[21]. The central wavelength and the peak transmission of the transparency window were 895 nm and 63%, respectively. This is in good agreement with the results calculated using the finite element method, as shown in Fig. 3(b). The transmission of the forbidden band was approximately 1%. Therefore, a high transmission contrast of 62% was achieved for the on-chip plasmon-induced transparency, which has increased four-fold when compared with previous reports[1–12,19]. To confirm the measured results, we also calculated the magnetic-field distributions of the plasmonic coupled nanocavities under excitation by CW incident light with wavelengths of 750 nm, 895 nm, and 955 nm using the finite element method, and the calculated results are shown in Fig. 3 (c) to (e), respectively. For the CW incident light at a wavelength of 750 nm (situated at a single transmission minimum), the magnetic-field distribution is mainly concentrated in the short nanocavity and no SPPs can propagate through the plasmonic waveguide, as shown in Fig. 3(c); this indicates that the resonance of the short nanocavity contributes a great deal to the generation of the plasmon-induced transparency. For the CW incident light at a wavelength of 895 nm (situated in the transmission peak), the magnetic-field distribution is mainly concentrated in both the long and the short nanocavities, and the SPPs can propagate through the plasmonic waveguide, as shown in Fig. 3(d); this indicates that the resonances of both the long and short nanocavities are related to the formation of the transparency window. For CW incident light at a wavelength of 950 nm (situated at the other transmission minimum), the magnetic-field distribution is mainly concentrated in the long nanocavity and no SPPs can propagate through the plasmonic waveguide, as shown in Fig. 3(e); this indicates that the resonance of the long nanocavity also contributes enormously to the generation of the plasmon-induced transparency. To further confirm the measured on-chip plasmon-induced transparency, we also calculated the transmission spectrum of the U-shaped plasmonic waveguide side-coupled to a single short (or long) stub nanocavity using the finite element method, and the measured results are as shown in Fig. 3(f). The single short (or long) stub nanocavity has the same structural parameters as the structure used in the plasmon-induced transparency sample. For the plasmonic waveguide that was side-coupled to the single stub nanocavity, a deep transmission valley appeared in the waveguide's transmission spectrum. Huang *et al.* have indicated that a single plasmonic stub nanocavity provides resonant surface plasmon modes with the magnetic-field distribution strongly confined within the stub region[25].

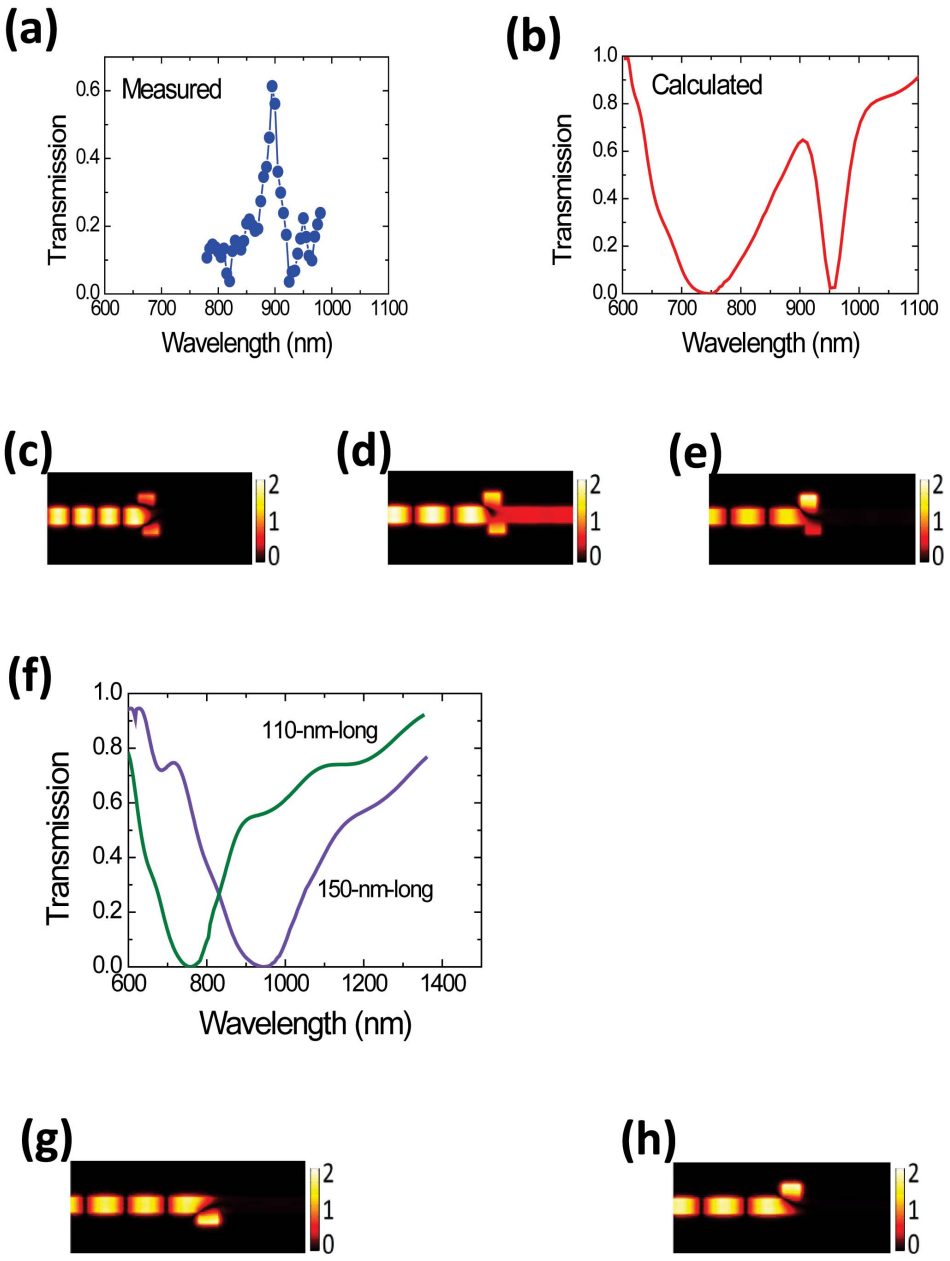

Figure 3 | Measured (a) and calculated (b) linear transmission spectra of the coupled nanocavities sample. Calculated magnetic-field distributions at wavelengths of 750 nm (c), 895 nm (d), and 950 nm (e) for the coupled nanocavities. (f) Calculated transmission spectrum of a U-shaped plasmonic waveguide side-coupled to a single 150-nm-long nanocavity (or to a single 110-nm-long nanocavity). Calculated magnetic-field distributions at a wavelength of 750 nm (g) for a single 110-nm-long nanocavity, and at wavelength of 955 nm (h) for a single 150-nm-long nanocavity.

For the plasmonic waveguide that was side-coupled to the plasmonic stub nanocavity, the energy of the guided SPP mode, which had a frequency in resonance with that of the nanocavity mode, will be coupled into the plasmonic stub nanocavity[26]. Accordingly, a deep valley appears in the transmission spectrum of the plasmonic waveguide, i.e., the transmission valley reflects the plasmonic nanocavity's resonance properties[26]. The resonant wavelength of the short stub nanocavity was located at 750 nm, which corresponds to the transmission minimum in the direction of the short wavelength of the on-chip plasmon-induced transparency, as shown in Fig. 3(b). We also calculated the magnetic-field distribution of the U-shaped plasmonic waveguide side-coupled to a single short stub nanocavity under excitation by 750 nm CW incident light using the finite element method, and the calculated results are shown in Fig. 3(g). The magnetic-field distribution was mainly confined within the stub nanocavity, and thus no SPPs can propagate through the plasmonic waveguide. This shows good agreement with the calculated magnetic-field distribution of the transmission minimum in the short-wavelength direction of the plasmon-induced transparency, as shown in Fig. 3(c). The resonant wavelength of the long stub nanocavity was located at 950 nm, which corresponds to the transmission minimum in the direction of the long wavelength of the on-chip plasmon-induced transparency, as shown in Fig. 3(b). We also calculated the magnetic-field distribution of the U-shaped plasmonic waveguide side-coupled to a single long stub nanocavity under excitation by 950 nm CW incident light using the finite element method, and the calculated results are as shown in Fig. 3(h). The magnetic-field distribution was mainly confined within the stub nanocavity, and thus no SPPs can propagate through the plasmonic waveguide, which shows good agreement with the calculated

magnetic-field distribution of the transmission minimum in the long-wavelength direction of the plasmon-induced transparency, as shown in Fig. 3(e). However, the transmission spectrum of the plasmonic coupled nanocavities used for the plasmon-induced transparency is not given by a simple superposition of the two single stub nanocavities. From Fig. 3(f), it can be found that the line width of the nanocavity mode was 98 nm for the short stub nanocavity and 183 nm for the long stub nanocavity. However, for the coupled nanocavities, the line width of the nanocavity mode was 214 nm for the short stub nanocavity and 48 nm for the long stub nanocavity. The broad (narrow) resonance is wider (sharper) than either of the individual resonances, which has been confirmed by the calculations of Verslegers *et al.*[21]. Also, the peak transmission of the plasmon-induced transparency at 63% was much larger than that at the intersection point of the transmission spectra of the single long and short stub nanocavities of 26%. This evidence confirms that the on-chip plasmon-induced transparency is caused by destructiveinterference between the two resonant excitation pathways involving the pair of long and short nanocavities.

To study the tunability of this on-chip plasmon-induced transparency, we measured the transmission spectrum of the plasmonic coupled-nanocavity pair sample when covered with different organic polymer layers, which were fabricated by the spin-coating method. Figure 4(a) depicts the measured transmission spectrum of the plasmonic coupled-nanocavity pair sample covered by an 80-nm-thick polymethyl methacrylate (PMMA) layer. A remarkable transparency window appeared in the transmission forbidden band, implying the generation of plasmon-induced transparency. The central wavelength of the transparency window was situated at 920 nm, indicating a 25 nm shift in the transparency window when compared with that of the plasmonic coupled-nanocavity pair in air. Also, the transmission at the center of the transparency window was as high as 63%. These measured results are in agreement with the results calculated using the finite element method, as shown in Fig. 4(b). The refractive index of PMMA was set at 1.49 in our calculations. Lukyanchuk *et al.* noted that the wavelength of the plasmonic resonance modes provided by the plasmonic nanostructures is heavily influenced by the refractive index of the ambient dielectric material[27]. A red shift in the resonant wavelength of the plasmonic modes provided by the plasmonic nanostructures can be achieved with an increase in the refractive index of the ambient dielectric material[28]. Figure 4(c) shows the measured transmission spectrum of the plasmonic coupled-nanocavity pair sample covered by an 80-nm-thick poly[(methyl methacrylate)-co-(disperse red 13 acrylate)] (PMMA-co-DR13) layer. Another remarkable transparency window appeared in the transmission forbidden band, which again implies the generation of the plasmon-induced transparency. The central wavelength of the transparency window was situated at 940 nm, indicating a 45 nm shift in the transparency window when compared with that of the coupled nanocavities in air. Also, the transmission at the center of the transparency window was as high as 62%. The measured results are in agreement with the results calculated using the finite element method, as shown in Fig. 4(d). The refractive index of PMMA-co-DR13 was set at 1.67 for our calculations. These results confirm the excellent tunability of the on-chip plasmon-induced transparency.

Discussion

Actively tunable on-chip plasmon-induced transparency has many potential applications in the fields of integrated photonic devices and integrated photonic chips based on plasmonic circuits. However, to date, no experimental progress has been reported in actively tunable on-chip plasmon-induced transparency. Many integrated photonic devices, including all-optical switches, all-optical routers, and all-optical memories, require low operating powers and ultrafast response times[7]. Ultrafast response times can be attained using an all-optical tuning method based on the third-order nonlinear optical

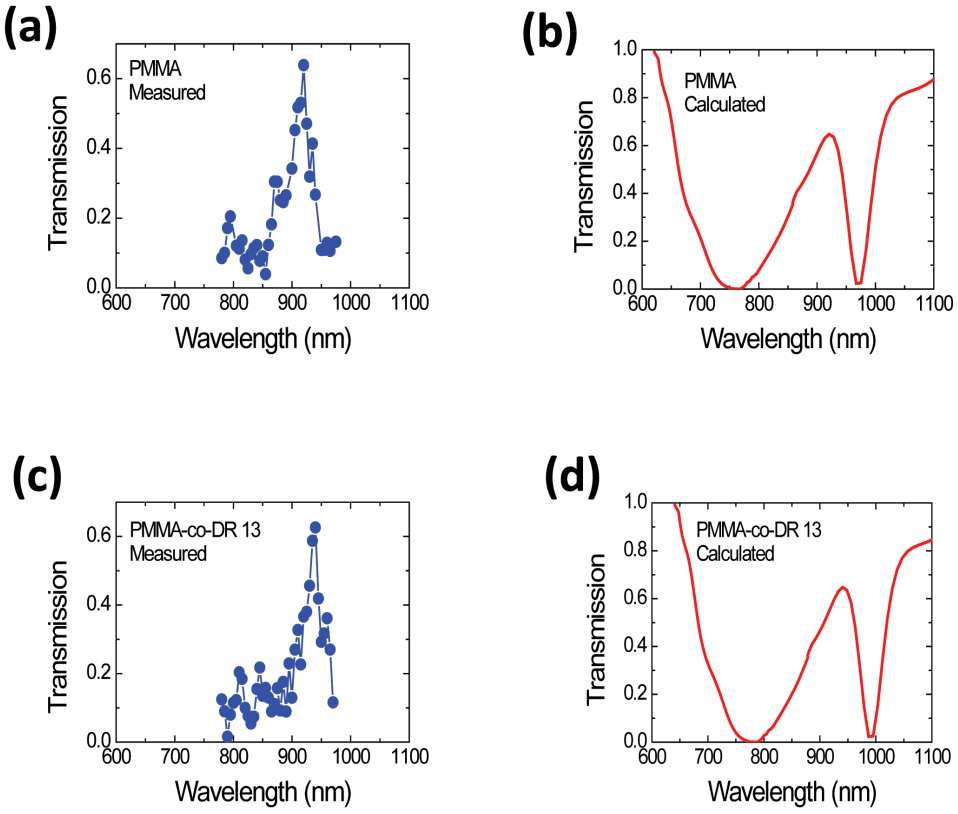

Figure 4 | Measured (a) and calculated (b) transmission spectra of the coupled nanocavities covered by an 80-nm-thick PMMA layer. Measured (c) and calculated (d) transmission spectra of the coupled nanocavities covered by an 80-nm-thick PMMA-co-DR 13 layer.

effect[7]. Graphene, which is a monolayer of carbon atoms arranged in a hexagonal two-dimensional crystal lattice, has flat linear absorption of approximately 2.3% across the entire visible and near-infrared range[28]. Therefore, enormously enhanced third-order optical nonlinearity can be expected in graphene because of its unique linear and massless band structure, i.e., interband optical transitions can occur at all photon energies[28]. Zhang *et al.* have noted that graphene has a giant nonlinear refractive index of $n_2 = -1.2 \times 10^{-7}$ cm^2/W in the visible and near-infrared range[29]. Nikolaenko *et al.* also noted that the fast carrier relaxation dynamics of graphene produced by carrier-carrier and carrier-photon interactions ensure an ultrafast response time of the order of 1 ps[30]. Therefore, graphene is an excellent nonlinear optical material with an ultrafast response time and high third-order optical nonlinearity. To study low-power and ultrafast all-optical tunable on-chip plasmon-induced transparency, we calculated the transmission spectrum of the plasmonic coupled-nanocavity pair covered by a single graphene layer under excitation by a pump light at a wavelength of 830 nm using the finite element method, and the calculated results are as shown in Fig. 5. The effective linear refractive index n_0 of graphene was set to be 2.4 in our calculations, as previously used by Kumar *et al.* in their experiments[31]. When the plasmonic coupled-nanocavity pair was covered by the single graphene layer, the central wavelength of the transparency window shifted to 1020 nm. The reason for this is that the presence of the graphene cover layer produces an enormous increment in the refractive index of the ambient dielectric surroundings. This has been confirmed by the measurements of Reckinger *et al.*[32]. Figure 5 shows very clearly that the transparency window shifts in the short-wavelength direction under excitation by 830 nm pump light. The effective refractive index n of graphene can be obtained based on the third-order nonlinear optical Kerr effect[33]:

$$n = n_0 + n_2 I \tag{1}$$

where $n_0 = 2.4$ and $n_2 = -1.2 \times 10^{-7}$ cm^2/W are the effective linear and nonlinear refractive indexes of graphene, respectively[29,31]. I is the intensity of the pump light. In our calculations, performed using the finite element method, the effective refractive index n of graphene is related to the pump intensity I based on equation (1). Therefore, the calculated transmission spectrum of the coupled-nanocavity pair covered by the single graphene layer under 830 nm pump light excitation at different intensities can be obtained. Because of the negative value of the effective nonlinear refractive index n_2, the effective linear refractive index n of graphene decreases under pump light excitation, which leads to a blue shift in the resonant wavelength of the plasmonic nanocavity pair. As a result, the central wavelength of the transparency window shifts in the short wavelength direction. When the pump intensity increased from zero to 5 MW/cm^2, the central wavelength of the transparency window shifted from 1020 nm to 950 nm. This implies that the transparency window can be continuously tuned over a wide wavelength range of 70 nm. The excellent all-optical tunability of graphene and the ultrafast all-optical tunable plasmonic resonance of plasmonic nanostructures covered by a graphene layer have also been confirmed by the measurements of Nikolaenko *et al.* and Hendry *et al.*[28,30]. These results confirm the perfect all-optical tunability of on-chip plasmon-induced transparency based on nanoscale plasmonic coupled nanocavities.

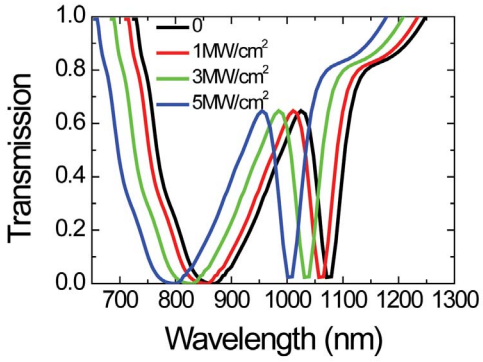

Figure 5 | Calculated transmission spectrum of the coupled nanocavities covered by a single graphene layer under excitation by 830-nm pump light at various intensities.

There are numerous advantages for on-chip plasmon-induced transparency based on nanoscale plasmonic coupled nanocavities, including direct on-chip applications in integrated photonic devices and integrated photonic circuits, concise structures, simple fabrication, convenient configuration tailoring, and the high transmission contrast between the transparency window and the stop band. In addition, enormously strong artificial modulation of signal light propagating on a chip can be realized using the plasmonic coupled nanocavities. This also provides a convenient basis for the study novel physical effects and phenomena related to strong interactions between light and matter.

In summary, we have realized on-chip plasmon-induced transparency based on nanoscale plasmonic coupled nanocavities. A high transmission contrast of more than 60% between the center of the transparency window and the stop band was obtained, which is a four-fold increase when compared with the results of previous reports. Wide tunability of the transparency window was also obtained through the use of different organic cover layers. Ultrafast all-optical tunable on-chip plasmon-induced transparency can also be realized through the excitation of a graphene cover layer by a pump light. This work not only paves the way for the realization of integrated photonic devices and quantum solid chips, but also provides a superior platform for the fundamental study of both nonlinear optics and quantum optics.

Methods

Sample fabrication. Films of 300 nm-thick gold were fabricated using a laser molecular beam epitaxy (LMBE) growth system (Model LMBE 450, SKY Company, China). We used the output beam (at a wavelength of 248 nm and with a pulse repetition rate of 5 Hz) from an excimer laser system (Model COMPexPro 205, Coherent Company, USA) as the excitation light source. The beam was focused on a gold target mounted on a rotating holder, located 15 mm away from the silicon dioxide substrates. The typical energy density of the excitation laser was approximately 450 mJ/cm^2. A focused ion-beam etching system (Model DB 235, FEI Company, USA) was used to prepare both the plasmonic waveguide and the stub nanocavities.

Nano-spectroscopy measurement setup. In the experiment, a nano-spectroscopy measurement system was used to measure the waveguiding properties of the plasmonic waveguide and the on-chip plasmon-induced transparency effects of the nanoscale coupled nanocavities. The nanoslit was normally illuminated from the back side using a p-polarized CW Ti:sapphire laser (Model Mira 900F, Coherent Company, USA) with different wavelengths. The optically-thick gold film can prevent direct transmission of the incident laser beam. The incident laser beam was focused to a spot with a radius of about 10 μm, with the center of the spot situated at a line parallel to the sample and reference waveguides. The vertical distance between the center of the spot and the plasmonic waveguide in the sample was equal to the distance between the center of the spot and the reference waveguide. This ensures uniform illumination of all the nanoslits in the entire sample and the reference waveguide. The line width of the laser spectrum curve was less than 1.5 nm, which ensures that only the required quasi-monochromatic SPPs can be excited by the nanoslits. The guided SPP mode was scattered by a decoupling grating that was etched in the output port of the plasmonic waveguide. The scattered light was collected by a long working distance objective (Mitutoyo 20, NA = 0.58), and then imaged using a charge-coupled device (CCD).

1. Kurter, C. *et al.* Classical analogue of electromagnetically induced transparency with a metal-superconductor hybrid metamaterials. *Phys. Rev. Lett.* **107**, 043901 (2011).
2. Papasimakis, N., Fedotov, V. A. & Zheludv, N. I. Metamaterial analog of electromagnetically induced transparency. *Phys. Rev. Lett.* **101**, 253903 (2008).
3. Zhang, S., Genov, D. A., Wang, Y., Liu, M. & Zhang, X. Plasmon-induced transparency in metamaterials. *Phys. Rev. Lett.* **101**, 047401 (2008).

4. Lu, Y. H. *et al*. Magnetic plasmon resonance: Underlying route to plasmonic electromagnetically induced transparency in metamaterials. *Phys. Rev. B* **82**, 195112 (2010).
5. Liu, N., Hentschel, M., Weiss, T., Alivisatos, A. P. & Giessen, H. Three-dimensional plasmon rulers. *Science* **332**, 1407 (2011).
6. Utikal, T. *et al*. Towards the origin of the nonlinear response in hybrid plasmonic systems. *Phys. Rev. Lett.* **106**, 133901 (2011).
7. Chai, Z. *et al*. Low-power and ultrafast all-optical tunable plasmon-induced transparency in plasmonic nanostructures. *Appl. Phys. Lett.* **102**, 201119 (2013).
8. Zhang, J. *et al*. Observation of ultra-narrow band plasmon induced transparency based on large-area hybrid plasmon-waveguide systems. *Appl. Phys. Lett.* **99**, 181120 (2011).
9. Yannopapas, V., Paspalakis, E. & Vitanov, N. V. Electromagnetically induced transparency and slow light in an array of metallic nanoparticles. *Phys. Rev. B* **80**, 035104 (2009).
10. Singh, R. *et al*. Observing metamaterial induced transparency in individual Fano resonators with broken symmetry. *Appl. Phys. Lett.* **99**, 201107 (2011).
11. Dong, Z. G., Ni, P. G., Zhu, J. & Zhang, X. Transparency window for the absorptive dipole resonance in a symmetry-reduced grating structure. *Opt. Express* **20**, 7206–7211 (2012).
12. Ooi, K., Okada, T. & Tanaka, K. Mimicking electromagnetically induced transparency by spoof surface plasmons. *Phys. Rev. B* **84**, 115405 (2011).
13. Kekatpure, R. D., Barnard, E. S., Cai, W. S. & Brongersma, M. L. Phase-coupled plasmon-induced transparency. *Phys. Rev. Lett.* **104**, 243902 (2010).
14. Chen, J. J., Wang, C., Zhang, R. & Xiao, J. H. Multiple plasmon-induced transparencies in coupled-resonator systems. *Opt. Lett.* **37**, 5133–5135 (2012).
15. Piao, X., Yu, S. & Park, N. Control of Fano asymmetry in plasmon induced transparency and its application to plasmonic waveguide modulator. *Opt. Express* **20**, 18994–18999 (2012).
16. Han, Z. & Bozhevolnyi, S. I. Plasmon-induced transparency with detuned ultracompact Fabry-Perot resonators in integrated plasmonic devices. *Opt. Express* **19**, 3251–3257 (2011).
17. Lu, H., Liu, X. M., Wang, G. X. & Mao, D. Tunable high-channel-count bandpass plasmonic filters based on an analogue of electromagnetically induced transparency. *Nanotechnology* **23**, 444003 (2012).
18. Tao, J. *et al*. Systematical research on characteristics of double-sided teeth-shaped nanoplasmonic waveguide filters. *J. Opt. Soc. Am. B* **27**, 323–327 (2010).
19. Han, Z. H., Ortiz, C. E. G., Radko, I. P. & Bozhevolnyi, S. I. Detuned-resonator induced transparency in dielectric-loaded plasmonic waveguides. *Opt. Lett.* **38**, 875–877 (2013).
20. Pile, D. F. P. *et al*. Theoretical and experimental investigation of strongly localized plasmons on triangular metal wedges for subwavelength waveguiding. *Appl. Phys. Lett.* **87**, 061106 (2005).
21. Verslegers, L., Yu, Z. F., Ruan, Z. C., Catrysse, P. B. & Fan, S. H. From electromagnetically induced transparency to superscattering with a single structure: a coupled-mode theory for doubly resonant structures. *Phys. Rev. Lett.* **108**, 083902 (2012).
22. Fu, Y. L. *et al*. All-optical logic gates based on nanoscale plasmonic slot waveguides. *Nano Lett.* **12**, 5784–5790 (2012).
23. Johnson, P. B. & Christy, R. W. Optical constants of the noble metals. *Phys. Rev. B* **6**, 4370–4379 (1972).
24. Li, X. E., Jiang, T., Shen, L. F. & Deng, X. H. Subwavelength guiding of channel plasmon polaritons by textured metallic grooves at telecom wavelengths. *Appl. Phys. Lett.* **102**, 031606 (2013).
25. Huang, Y., Min, C. J. & Veronis, G. Subwavelength slow-light waveguides based on a plasmonic analogue of electromagnetically induced transparency. *Appl. Phys. Lett.* **99**, 143117 (2011).
26. Noual, A., Akjouj, A., Pennec, Y., Gillet, J. N. & Rouhani, B. D. Modeling of two-dimensional nanoscale Y-bent plasmonic waveguides with cavities for demultiplexing of the telecommunication wavelengths. *New J. Phys.* **11**, 103020 (2009).
27. Lukyanchuk, B. *et al*. The Fano resonance in plasmonic nanostructures and metamaterials. *Nature Mater.* **9**, 707–715 (2010).
28. Hendry, E., Hale, P. J., Moger, J. & Savchenko, A. K. Coherent nonlinear optical response of Graphene. *Phys. Rev. Lett.* **105**, 097401 (2010).
29. Zhang, H. *et al*. Z-scan measurement of the nonlinear refractive index of graphene. *Opt. Lett.* **37**, 1856–1858 (2012).
30. Nikolaenko, A. E. *et al*. Nonlinear graphene metamaterial. *Appl. Phys. Lett.* **100**, 181109 (2012).
31. Kumar, N. *et al*. Third harmonic generation in graphene and few-layer graphite films. *Phys. Rev. B* **87**, 121406(R) (2013).
32. Reckinger, N., Vlad, A., Melinte, S., Colomer, J. F. & Sarrazin, M. Graphene-coated holey metal films: Tunable molecular sensing by surface plasmon resonance. *Appl. Phys. Lett.* **102**, 211108 (2013).
33. Boyd, R. W. *Nonlinear optics* (Academic Press, San Diego, 1992).

Acknowledgments

This work was supported by the National Key Basic Research Program of China under grants 2013CB328704 and 2014CB921003, the National Natural Science Foundation of China under grants 11225417, 11134001, 11121091, and 90921008, and the program for New Century Excellent Talents in University.

Author contributions

Z.Y. and X.H. proposed the idea. Z.Y., X.H. and H.Y. performed the measurements. Z.Y., X.H., H.Y. and Q.G. analyzed the data and co-wrote the manuscript.

Additional information

Competing financial interests: The authors declare no competing financial interests.

How to cite this article: Zhu, Y., Hu, X.Y., Yang, H. & Gong, Q.H. On-chip plasmon-induced transparency based on plasmonic coupled nanocavities. *Sci. Rep.* **4**, 3752; DOI:10.1038/srep03752 (2014).